Sequential Human Gait Classification With Distributed Radar Sensor Fusion

Haobo Li, *Member, IEEE*, Ajay Mehul, Julien Le Kernec, *Senior Member, IEEE*, Sevgi Z. Gurbuz, *Senior Member, IEEE*, and Francesco Fioranelli, *Senior Member, IEEE*

***Abstract*—This paper presents different information fusion approaches to classify human gait patterns and falls in a radar sensors network. The human gaits classified in this work are both individual and sequential, continuous gait collected by a FMCW radar and three UWB pulse radar placed at different spatial locations. Sequential gaits are those containing multiple gait styles performed one after the other, with natural transitions in between, including fall events developing from walking gait in some cases. The proposed information fusion approaches operate at signal and decision level. For the signal level combination, a simple trilateration algorithm is implemented on the range data from the 3 UWB radar sensors, achieving good classification results with the proposed Bi-LSTM (Bidirectional LSTM neural network) as classifier, without exploiting conventional micro-Doppler information. For the decision level fusion, the classification results of individual radars using the Bi-LSTM network are combined with a robust Naive Bayes Combiner (NBC), and this showed subsequent improvement compared to the single radar case thanks to multi-perspective views of the subjects. Compared to conventional SVM and Random Forest classifiers, the proposed approach yields +20% and +17% improvement in the classification accuracy of individual gaits for the range-only trilateration method and NBC decision fusion method, respectively. When classifying sequential gaits, the overall accuracy for the two proposed methods reaches 93% and 90%, with validation via a 'leaving one participant out' approach to test the robustness with subjects unknown to the network.**

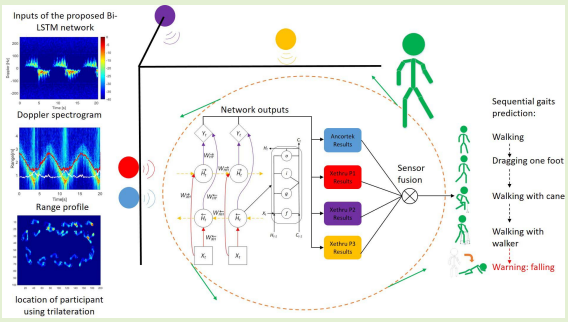

***Index Terms*— RF sensing, radar, machine learning, sensor fusion, gait analysis, fall detection.**

I. Introduction

NATIONAL health systems in many countries face significant challenges in providing comprehensive medical support to elderly people, for whom timely assistance after potentially life-threatening accidents, such as falls, heart attacks and stroke is crucial. For example, research showed that life expectancy after a fall is highly correlated with the timeliness of medical aide [1], and data from the U.S. Census Bureau showed that patients over 65 who have waited over an hour have a higher chance of death within the next 5 years than otherwise [1]–[3].

Changes in daily gait patterns and related metrics, such as gait asymmetry, imbalance, and slower or staggered gait with shorter stride, have been associated with increasing fall risk and health anomalies in older people [1], [4], [5]. Such symptoms could be very hard to detect at early stages, but may result in hospitalization or even emergency surgery when the situation worsens. Hence, a reliable fall detection [1] and health monitoring system capable of identifying daily gait patterns can be invaluable, not just for timely emergency response, but also to enable early intervention and treatment monitoring. More broadly, the recent COVID-19 pandemic has highlighted the relevance and benefits of remote monitoring technologies to reduce the need for physical proximity to diagnose and monitor a wide range of conditions that could potentially affect gait (e.g. concussion, stroke, and neuromuscular disorders). Contactless gait analysis technologies provide the opportunity to monitor the natural mobility of patients, as opposed to constrained settings typically used in hospitals or highly specialised laboratories. Moreover, less

Manuscript received November 25, 2020; revised December 19, 2020; accepted December 19, 2020. Date of publication December 24, 2020; date of current version February 17, 2021. This work was supported by the U.K. Engineering and Physical Sciences Research Council (EPSRC) under Grant EP/R041679/1 (INSHEP). The work of Haobo Li was supported by the University of Glasgow Mobility Scholarship through the research exchange to the University of Alabama. The associate editor coordinating the review of this article and approving it for publication was Prof. Piotr J. Samczynski. *(Corresponding author: Francesco Fioranelli.)*

Haobo Li and Julien Le Kernec are with the James Watt School of Engineering, University of Glasgow, Glasgow G12 8QQ, U.K. (e-mail: h.li.4@research.gla.ac.uk; julien.lekernec@glasgow.ac.uk).

Ajay Mehul is with the Department of Computer Science, University of Alabama, Tuscaloosa, AL 35487 USA (e-mail: aanbuselvam@crimson.ua.edu).

Sevgi Z. Gurbuz is with the Department of Electrical and Computer Engineering, University of Alabama, Tuscaloosa, AL 35487 USA (e-mail: szgurbuz@ua.edu).

Francesco Fioranelli is with the Microwave Sensing, Signals and Systems (MS3) Section, TU Delft, 2628 Delft, The Netherlands (e-mail: f.fioranelli@tudelft.nl).

Digital Object Identifier 10.1109/JSEN.2020.3046991

invasive technologies deployed in natural settings (e.g. private homes) can provide data more frequently and at less cost than evaluations conducted during hospital visits.

Towards these aims, radar has attracted much interest for human motion recognition [6], [7], especially in the applications of non-contact human activity classification, gesture recognition, and vital signs monitoring. Conventionally, wearable devices [3], [8] and video cameras [9] have been the focus for telemedicine research. Wearable devices are usually attached to the body (e.g. on the wrist, waist or ankle) via a strap, or placed in pockets or on the soles of shoes [8]. Examples include high resolution, multi-dimensional sensors to capture acceleration, angular speed or magnetic field strength to characterize different activities [8], or measurements of pulse, body skin temperature and humidity as vital signs [3]. However, wearable devices require user compliance to wear and carry them, and may be hindered by low battery life. For elderly people with cognition problems, this is risky, as the device could be forgotten or infrequently recharged. Video cameras [9] are contactless; however, the data presents potential privacy risks when used in personal settings, such as private homes.

In contrast, radar is a non-contact, remotely operable radio frequency (RF) device that is effective through-the-wall, in the dark, and does not measure any visual imagery that could violate privacy, even if hacked. While first developed for military applications, the advent of integrated RF transceivers has paved the way for miniaturized RF sensing systems [10], [11] that are now easily embedded into small hand-held devices, such as a cell phone or a smart watch.

The complex in-phase (I) and quadrature (Q) time stream provided by radar is typically converted into a 2D format using signal processing and time-frequency analysis. *Range maps* are a plot of the distance between the sensor and subject as a function of time, while the *micro-Doppler signature* reveals the variation of micro-Doppler with time [12]–[14]. The micro-Doppler signature is the pattern of multiple Doppler components generated by the different moving parts of the human body when performing activities, including walking gait. Unique movements result in unique patterns in the micro-Doppler signature, which are typically used as a basis for the recognition of activities (e.g. sitting, standing, bending, crawling, boxing, falls) or of different gaits (e.g. normal walking gait vs asymmetric, abnormal, or assisted gait).

Classification methods typically presented in the literature process the radar data as finite duration snapshots of a single activity or gait, without any natural transition from one activity to another, and with motion often constrained along a predefined direction with respect to the radar line of sight. The classification algorithms include conventional classifiers [15] (e.g. SVM, KNN, and Decision Trees), Auto-Encoders (AE) [16], Convolutional Neural Networks (CNNs) [17], [18], and Recurrent Neural Networks (RNNs) especially in their Long-Short Term Memory (LSTM) [19], [20] implementation or Stacked Gated Recurrent Units (SGRUs) [21].

Radar-based classification of activity sequences, i.e. sequences with natural transitions happening at any time between different actions of unconstrained duration, has not been adequately addressed in the literature. Stacked Recurrent GRUs have been proposed for sequential classification [21], [24], but the activity sequences were formed through concatenation, a process that introduces instantaneous and artificial transitions that are not present in natural sequences of human motion. With a different approach, a sliding window function that divides continuous data streams into smaller frames [25], [26] can be used. This does, however, increase the complexity of the approach as optimal window duration and overlap need to be found, and this values are likely to be strongly dependent on the specific dataset used for training.

In this paper, we address the problem of classification of sequential human gaits proposing a framework to exploit data fusion of range and micro-Doppler information extracted from multiple radar sensors in a network. The network consists of 3 Ultra Wide Band radar sensors operating at X-band and 1 FMCW radar operating at 24 GHz, enabling to test the effect of spatial position and operating frequency on the performance of the proposed approach. Together with conventional classifiers, the usage of Bi-LSTM (Bi-directional LSTM) networks is also investigated. These are suitable when forward and backward temporal dependencies between samples at separated time steps in a sequential data stream need to be learnt. This is useful in many applications, such as text, speech, natural language, and sound processing [22], [23]. For radar data of human activities or walking gaits in a sequence, Bi-LSTM can capture the kinematic constraints and correlations that link each action or gait to the previous and the following actions in the sequence. In previous work [27], [28], Bi-LSTMs were shown to be beneficial for classification of human activities and fall detection. However, in this paper we modify that approach. First, we analyse different types of gaits, which are inherently continuous and sequential movements unlike single actions like sitting, standing, etc. Then, we consider circular trajectories with changes of aspect angles with respect to the radar line of sight, unlike the constrained linear trajectories with zero aspect angle previously explored. Finally, in this work we do not only rely on micro-Doppler information, which is known to be most significant at zero aspect angle, but also consider range information from single radar and by fusing data from multiple radars.

To the best of our knowledge, the majority of research in the literature considered only walking gaits recorded as individual, "snapshot" data [4], [5], [29]. In this paper, we validate the proposed classification and fusion approaches first on individual gaits, and then on sequential gaits' sequences that include natural transitions between two or three types of gait, at times also followed by a fall event. Different sensor fusion schemes [30], [31] including signal combination, feature fusion, soft and hard decision level fusion [32] are investigated. Moreover, different types of input for the Bi-LSTM network are compared: range data, Doppler spectrograms, and fused range information via trilateration of the different radars in the network. The initial classification results suggest that the proposed approach outperforms conventional classifiers using feature selection, and that fusing the relevant information from the distributed radar sensors within the network is useful to achieve further improvement. Specific contributions include:

- Evaluation of the performance of the proposed classification and fusion approaches on realistic, continuous sequence of human gaits. The data stream contains natural transitions between different gait styles and the order of gaits is different in each repetition. Data fusion techniques including signal combination, feature fusion, soft and hard decision fusion have been utilized to improve the classification accuracy compared to single radar.
- Design of a novel trilateration algorithm to combine the range information from three identical radar sensors at different positions and use this as the temporal input to the Bi-LSTM classifier. We show that this algorithm can achieve similar performance to more conventional micro-Doppler information fusion with a relatively low computation load and processing time.
- Validation on a dataset with gait patterns from 14 participants and 12 different gait styles with multiple repetitions and varying aspect angles in circular trajectory. This allows us to validate the proposed approaches and compare the performance on a relatively large number of subjects and gait styles.

The remainder of this paper is organized as follows. Section II describes the radar network setup and the gait data collection. Section III presents the recognition of individual gait data using two conventional classifiers and the proposed Bi-LSTM network. Section IV validates the results of the approach applied to more challenging sequential gait analysis. Finally, section V concludes the paper and outlines possible directions for future work.

II. Experimental Setup

This section presents the experimental setup with details of the radar network used to collect data, and a description of the dataset.

A. Radar Network Setup

Gait measurements from a frequency modulated continuous wave (FMCW) radar at 25 GHz (Ancortek 2500B) and three ultra wide-band (UWB) impulse Doppler radars at 7.3 GHz (Novelda Xethru X4M300) were simultaneously recorded on a 2.7m×1.8m GaitRite mat embedded with pressure sensors in the Computational Intelligence for Radar (CI4R) Lab of the University of Alabama. The bandwidth of the FMCW radar and impulse radar were set at 2 GHz and 1.5 GHz, whereas the Pulse Repetition Interval (PRI) were fixed to 1ms and 2ms, respectively. The radars in the network were placed at three positions, shown in Fig. 1: in front of the participants, on the ceiling, and on the right hand side. This allows for simultaneous characterization of human gait patterns from three unique angles. The line-of-sight of different radar systems were carefully aligned to point the center of the scene to capture the strongest return. It should be also noted that the three UWB radars are separated and their positions was determined based on their azimuth beam-width (approximately 65 degrees), in order to minimize mutual interference and its effect on the subsequent classification processing.

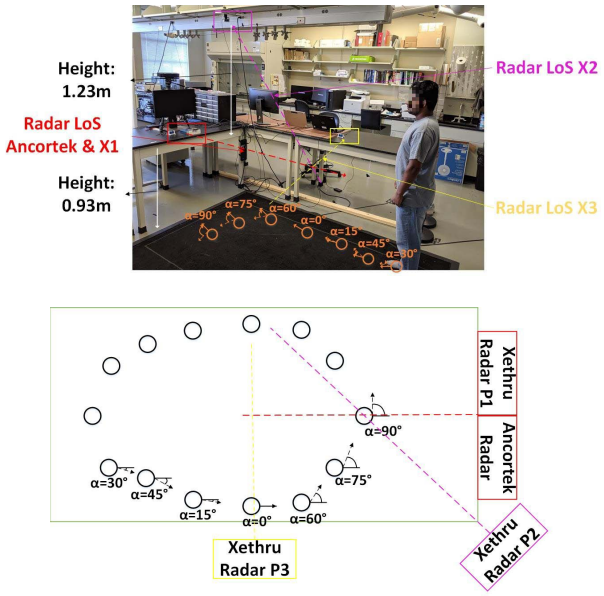

Fig. 1. 2D (bottom) and 3D (top) experimental setup including line-of-sights of different radar systems and walking trajectory (Red: radar in front of participants, Purple: radar on the ceiling, Yellow: radar on the right hand side).

The FMCW radar system utilizes a monostatic architecture with two horn antennas as the transmitter and receiver, whereas the two microstrip antennas of the impulse Doppler radar are fabricated with the signal generator and processor on one chip. The transmitted power are approximately 19 dBm and 4.1 dBm respectively.

B. Experiment Design and Data Collection

The dataset in this paper was collected involving 14 different participants with diversity in age (19-45), gender (3 female and 11 male), height (1.6 m to 1.85 m) and weight (60 kg to 95 kg). The gait and motion patterns performed are listed in Table I, where individual gait experiments involve gaits with ten distinctive styles and two different types of falling, and sequential gait experiments involve five different sequences of gaits (A-E in Table I). These gaits are proposed to simulate the scenario of walking at different velocities, dragging with one injured foot, falling and losing consciousness as well as rehabilitation from an accidental fall. To create more challenging classification scenario, pairs of potentially similar motions (e.g. walking with a cane and walking with a walker) are added to the list.

In the individual gait experiment, each gait was measured for a duration of 20 seconds independently for each participant. In the sequential gait experiments, five unique sequences of gaits are performed by the participants and acquired in an uninterrupted continuous fashion so that the data contains the natural transitions between different gaits. A total of 504 ($14 \times 12 \times 3$) for the individual gait experiments, whereas for the sequential gait experiments, a total of 71 observations were acquired (as not all participants were able to perform all the sequences).

TABLE I
LIST OF THE 12 INDIVIDUAL GAITS AND 5 (A-E) SEQUENTIAL GAITS, (T):GAIT TRANSITION, (F):FALLING

Individual gaits:
G1.Walking normally
G2.Walking quickly
G3.Walking slowly
G4.Dragging one foot
G5.Limping with a orthopedic cast
G6.Small steps
G7.Walking with a cane
G8.Walking with a walker
G9.Military walking
G10.Bunny jump
G11.Walking and direct fall
G12.Walking and controlled fall
Sequential gaits:
SeqA:20s G1 (T) 20s G3 (F) 5s controlled fall
SeqB:20s G1 (T) 20s G4 (F) 5s controlled fall
SeqC:20s G7 (F) 5s controlled fall
SeqD:20s G10 (T) 20s G1 (T) 20s G4
SeqE:20s G8 (T) 20s G3 (T) 20s G1

III. DATA PROCESSING FOR INDIVIDUAL GAITS

This section presents the analysis of the classification of individual gaits, at first using conventional classification algorithms based on supervised learning, and then Bi-LSTM networks.

A. Feature Fusion With Conventional Classifiers

Raw radar data contains hierarchical information [13], which can be used to measure range and velocity. Data from the FMCW radar can be mapped to the Range-Time domain with a Fast Fourier Transform (FFT), whereas the Doppler-Time domain or radar spectrogram is generated by performing a Short-Time Fourier Transform (STFT) on the range profiles. The STFT reveals the unique patterns of the micro-Doppler signature that stem from the rotations of the head and movements of the limbs and torso while walking. In this paper, spectrograms are computed for both FMCW and impulse radar data with a 0.2s Hamming window and an overlap of 95%. Fig. 2 illustrates the spectrograms acquired from six different walking gaits. Positive and negative Doppler frequencies [33], [34] are caused by reversal in net direction (towards/away) with respect to the radar. It may be observed that some pairs of gaits (e.g. walking and bunny jump, dragging one foot and walking with aid) present some similarities in terms of shape of radar envelope and Doppler amplitude.

Beyond the spectrograms, taking a further FFT along the time dimension or an IFT (Inverse Fourier Transform) on the logarithm of the spectrogram will create Cadence Velocity Diagram (CVD) and cepstrum respectively. These are different radar data domains that may contain additional information such as the cadence of walking and the gait frequency distribution. A total of 57 statistical features [15], [30], [35], summarized in Table II, are extracted from different radar data domains and supplied to the classifier. Specifically, 47 features from the radar spectrogram, 7 features from the CVD

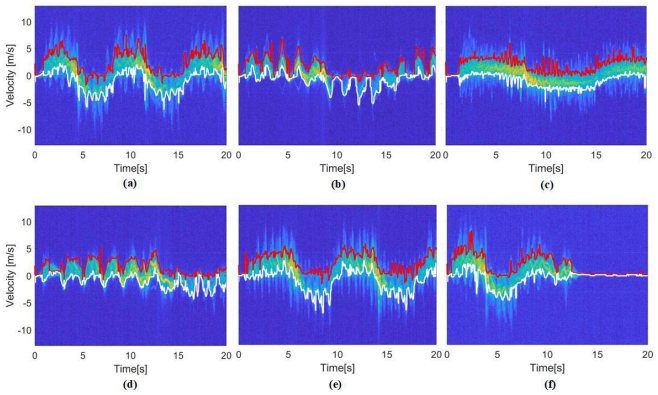

Fig. 2. Radar spectrogram: (a) walking (b) dragging a foot (c) small steps (d) walking with aid (e) bunny jump (f) walking and controlled fall; red line: upper envelope; white line: lower envelope.

TABLE II
LISTS OF THE RADAR FEATURES

Physical features from Doppler spectrogram	**#**
Mean, standard deviation, skewness, and kurtosis of the centroid of the Doppler spectrogram	4
Mean, standard deviation, skewness, and kurtosis of the bandwidth of the Doppler spectrogram	4
Two-dimensional mean, standard deviation, skewness, and kurtosis of the whole segment of the spectrogram	4
Mean, maximum and minimum of the upper envelope	3
Mean, maximum and minimum of the lower envelope	3
Difference between mean of the upper and lower envelope	1
Transform-based features from Doppler spectrogram	**#**
Mean and standard deviation of the first left and right eigenvector of the SVD decomposition of the spectrogram	4
Sum of pixels of the entire left and right matrices	2
Mean of the diagonal of the left and right matrices	2
DCT of the spectrogram	10
First 10 coefficients of the LPC of the spectrogram	10
Features from CVD profile	**#**
Step repetition frequency	1
Step repetition frequency band peak	2
Intensity of main peak in CVD	1
Maximum of the main peak	1
Energy of the main peak	1
Most significant Doppler frequency in CVD	1
Features from radar cepstrum	**#**
Maximum, minimum and mean of the cepstrum	3
Total numbers	**57**

[4], [5] and 3 features from the cepstrum [36], [37] are extracted. This selection of different features from different works in the literature is expected to increase the diversity and the overall relevant information for gait classification. Doppler centroid and bandwidth describe the position of the central mass of the human body in the walking period and the energy surrounding this. Step repetition frequency is the most significant feature from the CVD domain as it is shown to be associated with gait patterns [4], whereas the cepstral coefficients are considered as an additional source of information to characterize the periodicity of movements, thus we select three features from them (maximum, minimum and mean) to complement the features extracted from the other radar domains. Additionally, all the feature vectors are

normalized by subtracting the mean and dividing by the standard deviation.

Linear Support Vector Machine (SVM) [15], [31] and Random-Forest Bagging (RFB) [38] classifier with 200 trees are chosen as conventional classifiers to distinguish the individual gaits. SVM constructs a hyper-plane between the predictors to separate them, whereas RFB algorithm selects a stochastic subset of predictors to train at each decision split of the trees. The advantage of conventional classifiers with respect to more complicated neural networks is their relatively small computational load with still acceptable performance.

In the real-world, the pre-trained classifier needs to be able to cope with data from new users, so it is significant to consider and simulate this circumstance. Hence, 'Leaving One participant Out' (L1O) cross-validation method is used to separate the data into training and testing set, where data from one of the participants is selected for evaluating the performance and all others are used for training the classification model. The training and testing iteration will continue until each participant is tested upon, and average performance can then be investigated.

Information fusion can improve the classification performance in our radar network as diverse information from multiple radar sensors can be combined. This can be particularly advantageous when the micro-Doppler information from one (or more) sensors is poor due to unfavourable aspect angles between the movement trajectory and the radar line of sight. In our case, given the location of the sensors and the elliptic trajectory of the participants' walking gaits, there are areas where a specific radar can only see tangential movements with respect to the line of sight, i.e. not much Doppler information. Feature level fusion can be accomplished by constructing a wider feature pool derived by combining features obtained from all RF sensors. The feature matrix of one single RF sensor, F_{Radar} is defined as

$$F_{Radar} = \begin{bmatrix} F_{11} & F_{12} & F_{13} & \dots & F_{1j} \\ F_{21} & F_{22} & F_{23} & \dots & F_{2j} \\ \vdots & \vdots & \vdots & \vdots & \vdots \\ F_{i1} & F_{i2} & F_{i3} & \dots & F_{ij} \end{bmatrix} \tag{1}$$

where j is the number of features extracted from each sensor and i is an index for each labelled data sample collected by that radar. Through feature fusion a larger matrix can be constructed by horizontal concatenation of the matrices of each radar considered in the network, such as

$$F_{Fusion} = [F_{Radar1} \quad F_{Radar2} \quad \dots \quad F_{RadarK}] \tag{2}$$

where K indicates the number of radar sensors whose individual feature matrices are combined together.

Soft decision fusion [30] can be formulated as

$$\begin{aligned} S_{Fus}(n,c) = W_{An} \cdot S_{An}(n,c) + W_{X1} \cdot S_{X1}(n,c) \\ + W_{X2} \cdot S_{X2}(n,c) + W_{X3} \cdot S_{X3}(n,c) \end{aligned} \tag{3}$$

where the posterior probability of each class is generated to indicate the confidence level of the classifier making decisions. S_{An}, S_{X1}, S_{X2}, S_{X3} and S_{Fus} are the probability matrix for each individual radar and fusion cases; n denotes the observation; c refers to the class. W_{An}, W_{X1}, W_{X2}, W_{X3} represent the sensor weight of different radars in the fusion procedure: a radar with better performance is associated with higher weight. In our case, all the weight indexes are equal to 1. The probability matrix from each radar sensor is accumulated to a new score matrix, where the new prediction label is the class yielding the highest fusion posterior probability. This procedure can help correct events misclassified by single radar and ultimately yield higher confidence level for the correct class after fusion.

Hard decision fusion [27], [39] utilizes the prediction results of the classifier in the confusion matrices, rather than focusing on the posterior probabilities. Typical hard fusion methods include majority voting (MV), weighted majority voting (WMV), Recall Combiner (RC) and Naive Bayes Combiner (NBC) [39]. In our previous work [27], it was shown that NBC outperformed other hard fusion methods, and this was chosen to be the hard fusion approach also in this paper. Compared to soft fusion, NBC attempts to gather the results from all the N classifiers to build a classifier ensemble. C_k is the class of interest, d is a class set containing all the classes to distinguish, $P(C_k|d)$ is the probability that class C_k is chosen from the class set d to become the output class and $P(C_k)$ denotes the supporting rate for class C_k in the classifier ensemble. R_m is the prediction result of classifier m from classifier ensemble, whereas $p_{m,R_m,k}$ refers to the confusion matrix element p for classifier m, row R_m and column k. It is observed that $p_{m,R_m,k}$ is highly correlated with the classification performance of classifier m, as the confusion matrix is computed based on its predictions. Therefore, if one radar sensor (e.g. Ancortek FMCW radar) outperforms the other radars in classifying a specific subset of classes, then such radar will have higher impact than the others on the final decision after fusion. In this way, hard fusion emphasizes and exploits the strong points of each radar, and generally yields better performance than soft fusion.

$$P(C_k|d) = P(C_k) \cdot \prod_{m=1}^{N} p_{m,R_m,k} \tag{4}$$

However, some of the features in the feature set are redundant for classification. Feature selection techniques [30], [35] are typically utilized to pick the most effective subset of features from the original feature set. Feature selection algorithms include F-score [30], Relief-F [30], and sequential forward/backward selection [30], [35]. Generally, wrapper methods, such as sequential feature selection, outperform F-score and Relief-F by leveraging computational power to test each possible feature combination in combination with the chosen classifier. In this paper, sequential backward selection (SBS) is chosen as the selected feature selection approach, where features are eliminated one by one from the entire set until the maximum classification accuracy is achieved. In our case, compared to forward selection, backward selection algorithm converges more quickly since it avoids starting with a small feature set.

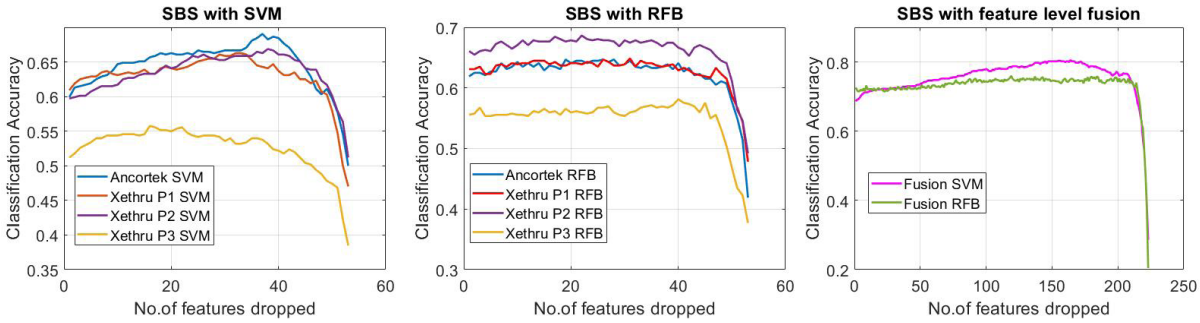

Fig. 3. The classification accuracy as a function of the number of features dropped via SBS algorithm: (a) with SVM classifier on individual radar data, (b) with RFB classifier on individual radar data, and (c) with both SVM and RFB on feature fusion of all four radar.

Fig. 3 shows the dependence of classification accuracy on the number of features dropped during the SBS procedure. In the case of using the SVM classifier as part of the SBS, the FMCW Ancortek radar outperforms the other radars with a maximum 69% classification accuracy achieved when 20 features are used (37 features dropped from the original set of 57 features). In the case of Xethru P1-P3 radars, with SBS they gain +4.5% to +7% accuracy improvement with respect to the case of using all features. Compared to SVM, using SBS algorithm with a RFB classifier is less effective, as the maximum accuracy increases only of +2-3% with respect to the performance using all features. RFB is an ensemble of decision trees which integrates preliminary feature selection, whereas the SBS basically filters the features again and as a result of that, the improvement is not as significant as SBS-SVM. When feature fusion is used, the SBS with RFB and SVM classifier show an accuracy improvement of +3.3% and +12% with 109 and 64 features respectively used, compared to using the whole set of 228 features. The best classification result using L1PO cross-validation after feature fusion reaches 80.56%.

B. Bi-LSTM Recurrent Neural Network Structure

In this sub-section we introduce the Bi-LSTM network used as classifier of sequential walking data. The network contains an input layer, two Bi-LSTM layers, a softmax layer and a classification layer. The network is capable of learning the forward and backward time dependencies through characterizing and memorizing the possible correlations within the sequence of the data [22], [40]. For individual gaits, due to repetitive actions, such as arm and leg swing, the network can extract the common temporal features between those periodic gait patterns. For sequential gaits, the network is able to learn the dependencies related to the order of the gaits, where the transition between two different gait styles is the key to reinforce the inter-connections among the cells on two Bi-LSTM layers. A dual layer architecture has higher capabilities than a single layer one; however, there is a trade off between the number of layers and the computational complexity to achieve a boost in accuracy with feasible network training time, as shown in previous work [27], [28].

The hyper-parameters of the network training are listed in Table III. The hyper-parameters are fine-tuned to achieve the best test performance for the different types of inputs data considered in this paper, namely sequential information extracted from the micro-Doppler of single radar, information extracted from the range-time matrix of single radar, and information generated by combining the range information of multiple radar through trilateration. The max epochs for the network training using range information is doubled compared to the training using Doppler and trilateration location information. This accounts for the slower conversion of the network when range information from single radar is used.

TABLE III
THE HYPER-PARAMETERS FOR THE BI-LSTM NETWORKS PROPOSED IN THIS PAPER

HYPER-PARAMETERS	Micro-Doppler single radar Input	Range-Time single radar input	Range tri-lateration multiple radar input
Number of inputs	4	2	2
Number of classes	12		
Training and testing scheme	L1PO (Leaving one participant out)		
Mini batch size	8		
Max Epochs	200	400	200
Initial learning rate	1e-3		
Learning rate drop period	50	100	50
Learning rate drop factor	0.1		
Optimization function	Adam		

The connections and weight transfer between the layers in the proposed network along with the inter-links of gates of the Bi-LSTM cell are sketched in Fig. 4.

The sequential forward operation of a Bi-LSTM cell is controlled by

$$\overrightarrow{H}_t = \sigma(W_{\overrightarrow{XH}} X_t + W_{\overrightarrow{HH}} \overrightarrow{H}_{t+1} + b_{\overrightarrow{H}}), \tag{5}$$

while the backward operation of the cell is governed by

$$\overleftarrow{H}_t = \sigma(W_{\overleftarrow{XH}} X_t + W_{\overleftarrow{HH}} \overleftarrow{H}_{t+1} + b_{\overleftarrow{H}}). \tag{6}$$

The output is given by summing the product of the weight and hidden state with the bias; namely,

$$Y_t = W_{\overrightarrow{HY}} \overrightarrow{H}_t + W_{\overleftarrow{HY}} \overleftarrow{H}_t + b_Y \tag{7}$$

where σ is the *tanh* activation function, X_t is the input of the neural network, H_t with an arrow on its head indicates the

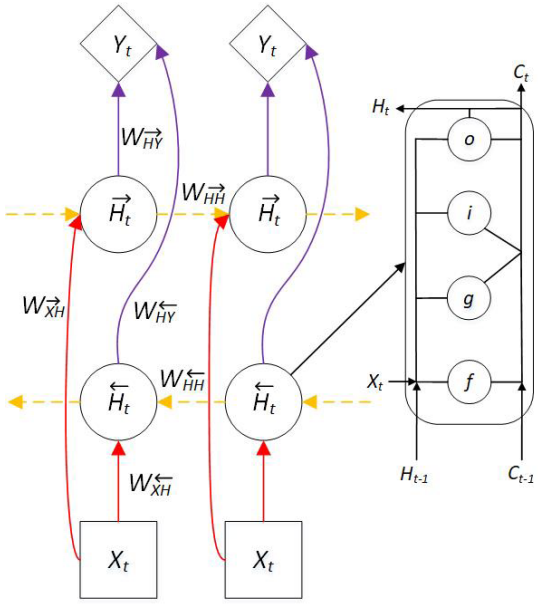

Fig. 4. Structure of the Bi-LSTM layers in the proposed network and sketch of a single LSTM cell.

hidden state with forward/backward direction, W_{ab} shows the weights associated with hidden states and I/O, b_n is the bias component and Y_t is the network output.

The information propagation between the layers and hidden cells are sketched in different color arrows. Inside the Bi-LSTM hidden cell, the *forgot* gate f can reset the cell state by removing the unnecessary prior knowledge from the previous cell state (C_{t-1}). The *cell candidate* g is the key element which computes the new memorable information. The *input* gate i decides whether the input (X_t) is important to be sent to the cell candidate for next step computing. The *output* gate o controls the amount of current cell state (C_t) to be exposed. Finally the output cell state will be added with the previous hidden state (H_{t-1}) to form the current hidden state (H_t). The detailed equations of working states into each gate can be found in [22], [40].

C. Results With Bi-LSTM Networks

In this section, the classification results of individual gaits described in Table I (G1 to G12) using different types of inputs to the Bi-LSTM networks are discussed; notably these are micro-Doppler information, range-time information, and signal level combination of multiple radar with trilateration.

1) Decision Fusion With Bi-LSTM Networks: Doppler centroid and bandwidth are firstly generated from the micro-Doppler spectrogram. Then the upper and lower envelope are also extracted. These four different types of features are utilized as parallel inputs to the proposed Bi-LSTM network, referred to as *Doppler Bi-LSTM*. Centroid and bandwidth represent the centre of mass of the human body and the Doppler spread around this respectively, whereas the upper and lower envelopes of the micro-Doppler signature reflect the variation in the velocity of human limbs (e.g. arms and legs) that swing during the walking gait. These features are successfully implemented in other applications, such as arms motion detection and gesture recognition [42], [43].

Fig. 5 shows the *Doppler Bi-LSTM* classification results for each participant through the L1PO training and testing scheme. All the four radar sensors used in isolation yield similar mean classification accuracy between 88% and 92%, but with higher variability in terms of the minimum accuracy (i.e. the participant whose testing results yielded the lowest accuracy). There is significant variability of the performance for a given participant when using different radar systems, either if the radar are co-located but operating at different frequency (e.g. participant #3 and #4 for Ancortek and Xethru P1), or if they are the same radar but located at different places (e.g. participant #2 for the three Xethru P1-P2-P3). When fusion based on Naive Bayes Combiner across the four radar is used, all the performance metrics are improved, not only in terms of mean (98.2%) and minimum (94.6%) accuracy among participants, but also in terms of the standard deviation among the 14 participants that is significantly reduced.

Fig. 6 characterises the prediction results of the *Doppler Bi-LSTM* network with respect to the aspect angle. As the participants walk along the elliptical trajectory, this angle changes with different values across the different radar sensors in the network. At high aspect angle, it is expected that the Doppler signature will be attenuated, potentially compromising the classification results. In this test shown in this figure, the recordings of the 12 individual gaits of a participant are cascaded one after the other to generate a 240 s long sequence (12 gaits, with 20 s recording for each individual gait) that is processed by the network. A number of wrong classifications, indicated by the orange prediction line on “False”, can be seen in different moments for the different radar sensors used in isolation. This happens more frequently with the Ancortek radar and with the Xethru P2, mostly in the period between 120 and 160s. Using fusion, the number of false predictions can be significantly reduced by leveraging the advantages of each sensor, assuming that at any given moment at least one of the radars in the network will have low aspect angle view on the target, leading to favourable Doppler.

Fig. 7 shows the confusion matrix with the results for individual gaits in Table I obtained with fusion. Rows and columns represent the target and output classes, while the diagonal elements are the events correctly classified and non-diagonal elements indicate the misclassified gaits. Most of the classes have a nearly perfect recognition rate, whereas some confusion occurs between ’normal walking’, ’walking and direct fall’ and ’walking and controlled fall.’ This is due to participants experiencing some hesitation or delay prior to performing the fall.

2) Signal Combination With Bi-LSTM Networks: In the previous section, we discussed the use of information extracted from micro-Doppler spectrograms as inputs to the Bi-LSTM network. However, generating spectrograms requires an extra step of processing from range information. Thus, it is interesting to explore whether comparable performance could be achieved directly using range information into the Bi-LSTM network. Fig. 8 shows range-time maps for different gaits, where the red and white solid lines denote the average distance

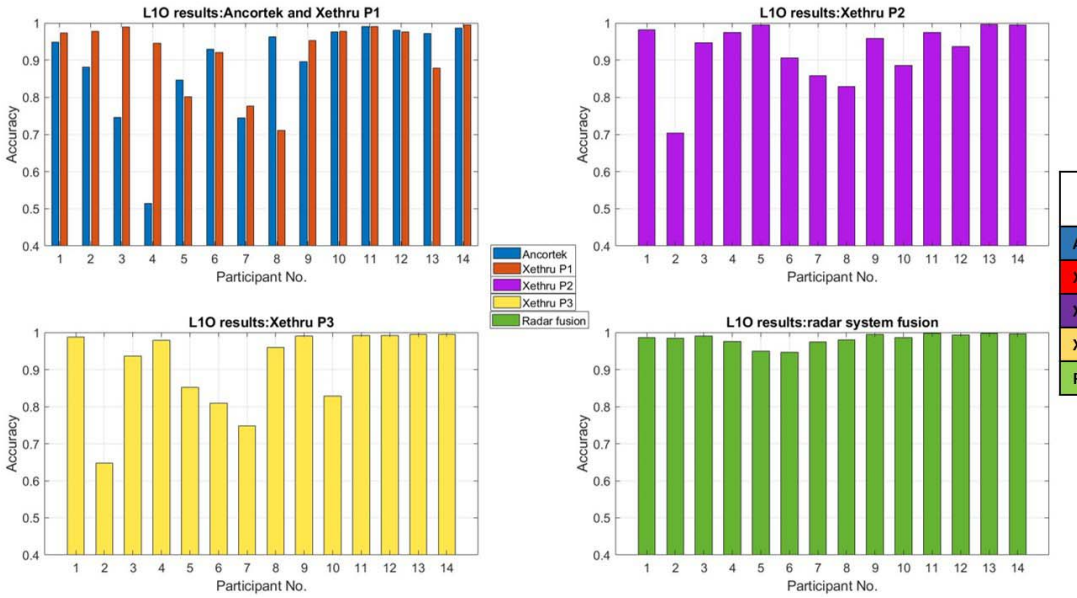

	Mean Acc(%):	Min Acc(%):	STD(%):
An	88.4	51.4	13.49
X1	91.9	71.1	9.19
X2	92.4	70.4	8.27
X3	90.8	64.8	11.2
Fus	98.2	94.6	2.18

Fig. 5. The classification performance of the Doppler Bi-LSTM with single radar and fusion for *individual gait data*. Different colours indicate results from the different radar sensors used in isolation or with fusion (green).

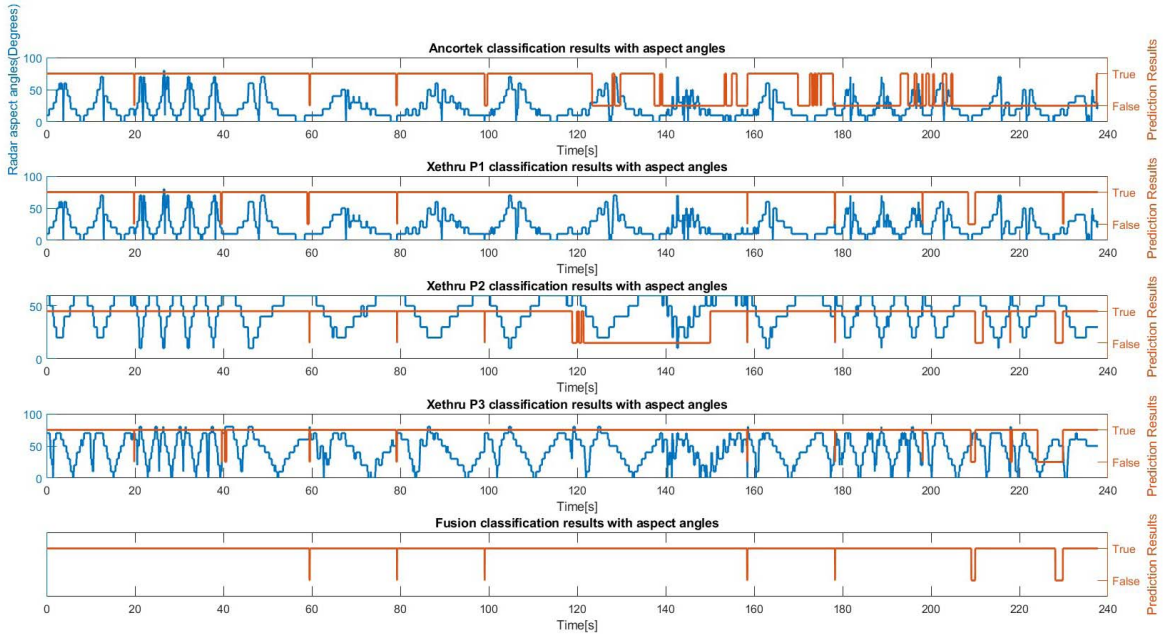

Fig. 6. The prediction results of the Doppler Bi-LSTM network with respect to the aspect angle for *individual gait data*. From top bottom: Ancortek, Xethru P1, P2, P3, and radar fusion. Aspect angle values reported in blue; network prediction results as binary true-false values in orange.

between radar and centre of mass of the subject's signature, and the range extent along the profile due to movements of arms and legs during the gait. These two features, average distance and range extent, are computed from the Range-Time matrix in the same way as Doppler centroid and bandwidth from the spectrogram [44], and then used as inputs to the network. The recorded target signal strength is between 0 and approximately -25 dB in the normalised plots, indicated by red to light blue in the colormap. Background noise is shown in dark blue, at about -30dB and below. The difference between the range-time plots of different gaits is not as immediately noticeable as differences in the spectrograms were. However, classification based on range maps, if successful, can save the computational effort of extracting micro-Doppler, which can be relevant for portable devices with limited memory and computational capacity.

As a further approach to use range only information, a trilateration algorithm is applied to fuse the information on the range to the participant from the three Xethru radar sensors. The geometry of the sensors relative to the subject and the resulting ranges are sketched in Fig. 9, where x and y are the coordinate of the subject. Mathematically, these ranges can be

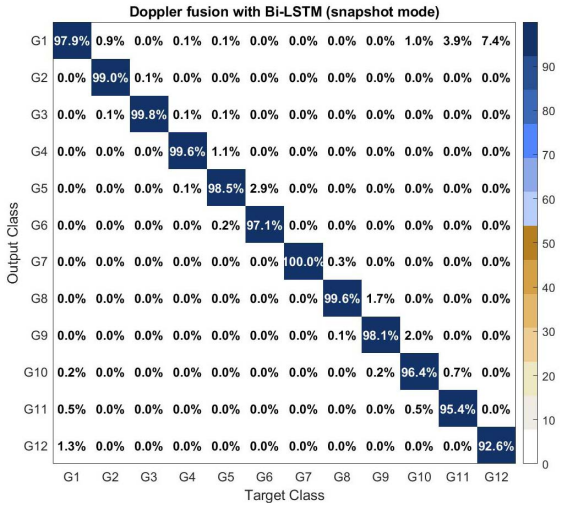

Fig. 7. Confusion matrix of Doppler Bi-LSTM fusion using a NBC for *individual gait data*.

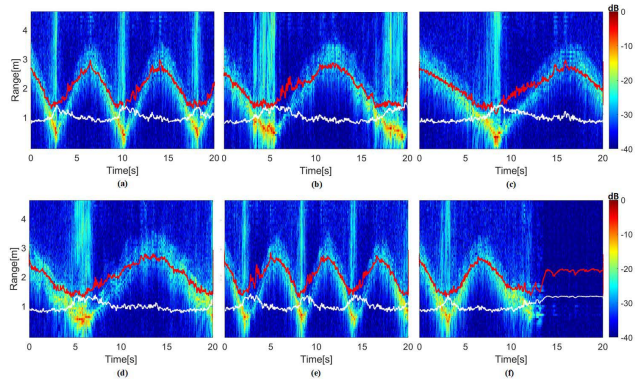

Fig. 8. Range-time maps for several gaits: (a) walking; (b) dragging foot; (c) small steps; (d) walking with aid; (e) bunny jump; (f) walking and controlled fall. Red line: average radar-subject distance. White line: range extent around average value.

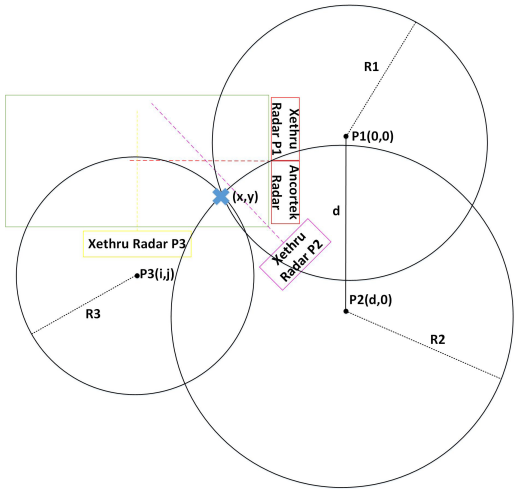

Fig. 9. Concept figure of trilateration algorithm: Xethru P1 (0,0); Xethru P2 (d,0); Xethru P3 (i,j)); R1(distance from Xethru P1 to participant); R2(distance from Xethru P2 to participant); R3(distance from Xethru P3 to participant).

computed as three circumferences as

$$R_1^2 = x^2 + y^2 \tag{8}$$

$$R_2^2 = (x-d)^2 + y^2 \tag{9}$$

$$R_3^2 = (x-i)^2 + (y-j)^2 \tag{10}$$

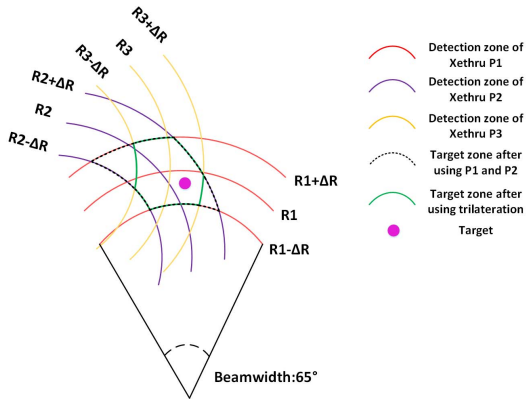

Fig. 10. Sketch of trilateration advantage in localising the subject.

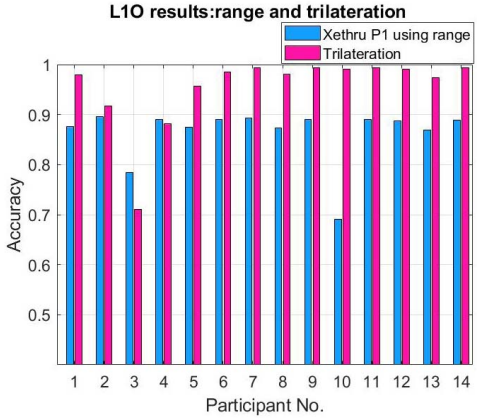

Fig. 11. Classification accuracy for range only information from Xethru P1 and trilateration for *individual gait data*.

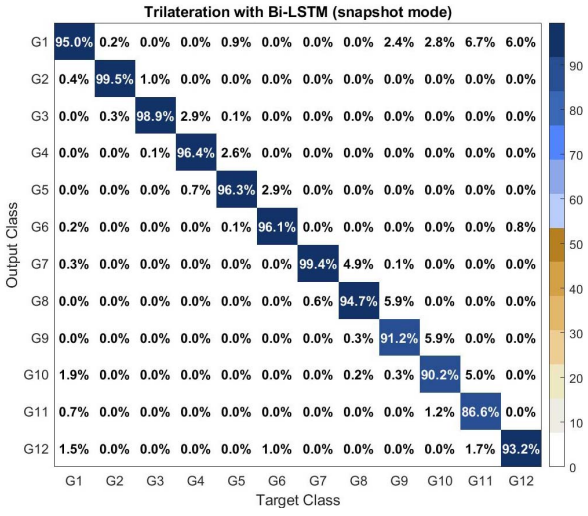

Fig. 12. Confusion matrix of information fusion using multiradar trilateration for *individual gait data*.

where x is

$$x = (R1^2 - R2^2 + d^2)/2d \tag{11}$$

and y is

$$y = (R1^2 - R3^2 - x^2 + (x-i)^2 + j^2)/2j \tag{12}$$

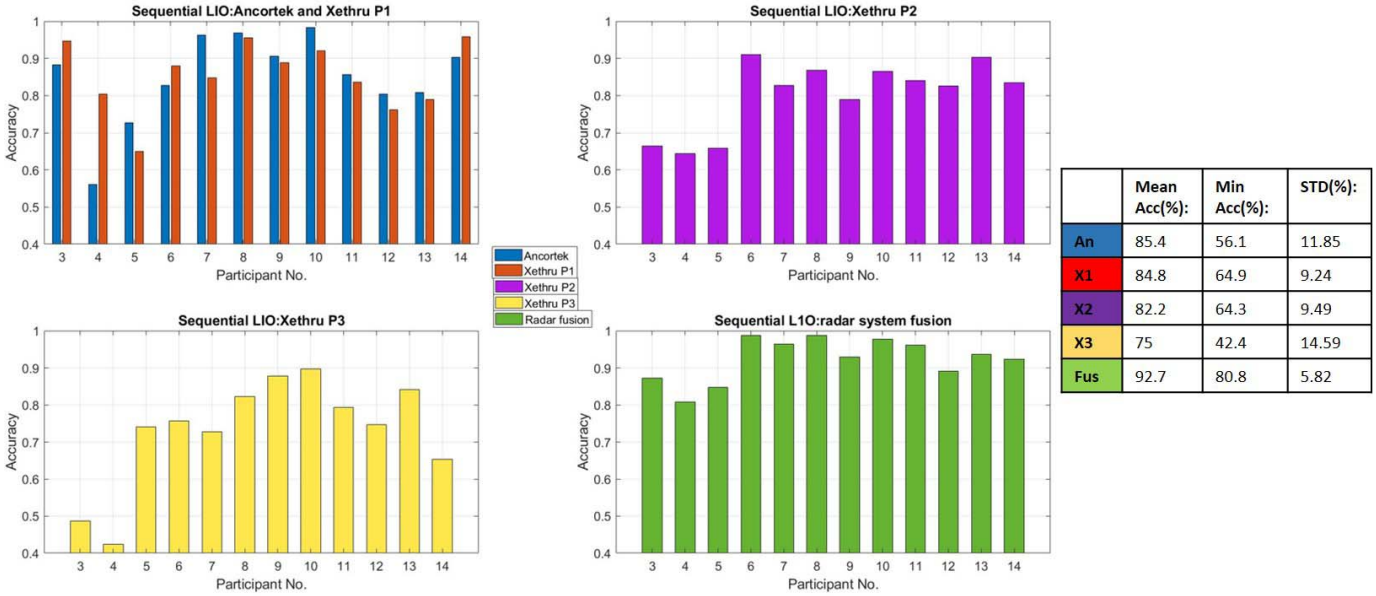

	Mean Acc(%):	Min Acc(%):	STD(%):
An	85.4	56.1	11.85
X1	84.8	64.9	9.24
X2	82.2	64.3	9.49
X3	75	42.4	14.59
Fus	92.7	80.8	5.82

Fig. 13. The classification performance of the Doppler Bi-LSTM with single radar and fusion for *sequential gait data*. Different colours indicate results from the different radar sensors used in isolation or with fusion (green).

In our case, as the Xethru P2 is installed on the ceiling of the lab, rather than directly using R_2 as given above, the length of its projection on the 2-D horizontal plane is considered as the actual value. The x and y coordinates of the participant are then extracted and utilized as the two inputs to the Bi-LSTM network. In comparison to the range information from each individual RF sensor, trilateration decreases the variance level in the measurement errors of single radar by a factor of N equal to the number of sensors [45], where in our case, $N = 3$. Moreover, using the geometry of the radar, it is also possible to explain why the trilateration-based signal level fusion can improve the classification accuracy. As shown in Fig. 10, each radar sensor has a range resolution R, thus the target location would be at the estimated measured distance plus/minus R. As the single-receiver radars have no angular resolutions, the target could appear anywhere within the radar beam-width, approximately 65 degrees. By using the range information of two radar sensors, namely, Xethru P1 and P2 (UWB radar in front of the participants and on the ceiling), the target location can be narrowed to one small area (marked in black dash line); this small area can be subsequently narrowed by using trilateration (marked in green solid line). Compared to using range measurements of single radar, trilateration-based signal level fusion algorithm can increase the precision of localization, which is beneficial to the following training and testing of the proposed Bi-LSTM network. The computational cost for applying trilateration on the range data is much lower than Doppler processing plus further decision level fusion: the running time is 90% less using MATLAB implementation on the same computer.

Fig. 11 compares the results of using range only data from Xethru P1 with those from trilateration, both with L1PO cross validation. The average classification accuracy are 84.4% and 95.3% for range information from Xethru P1 and multi-radar localization information by trilateration. Compared

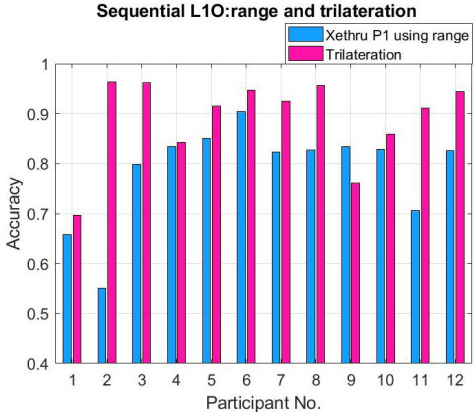

Fig. 14. Classification accuracy for range only information from Xethru P1 and trilateration for *sequential gait data*.

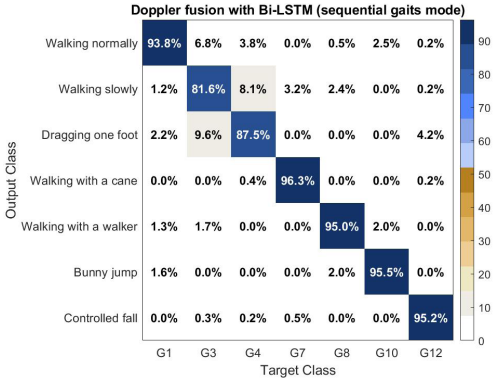

Fig. 15. Confusion matrix of Doppler Bi-LSTM fusion using a NBC for *sequential gait data*.

to the micro-Doppler classification using Xethru P1 in Fig. 5, range only results report an accuracy drop of approximately 7.5%, whereas a boost in accuracy between +2%

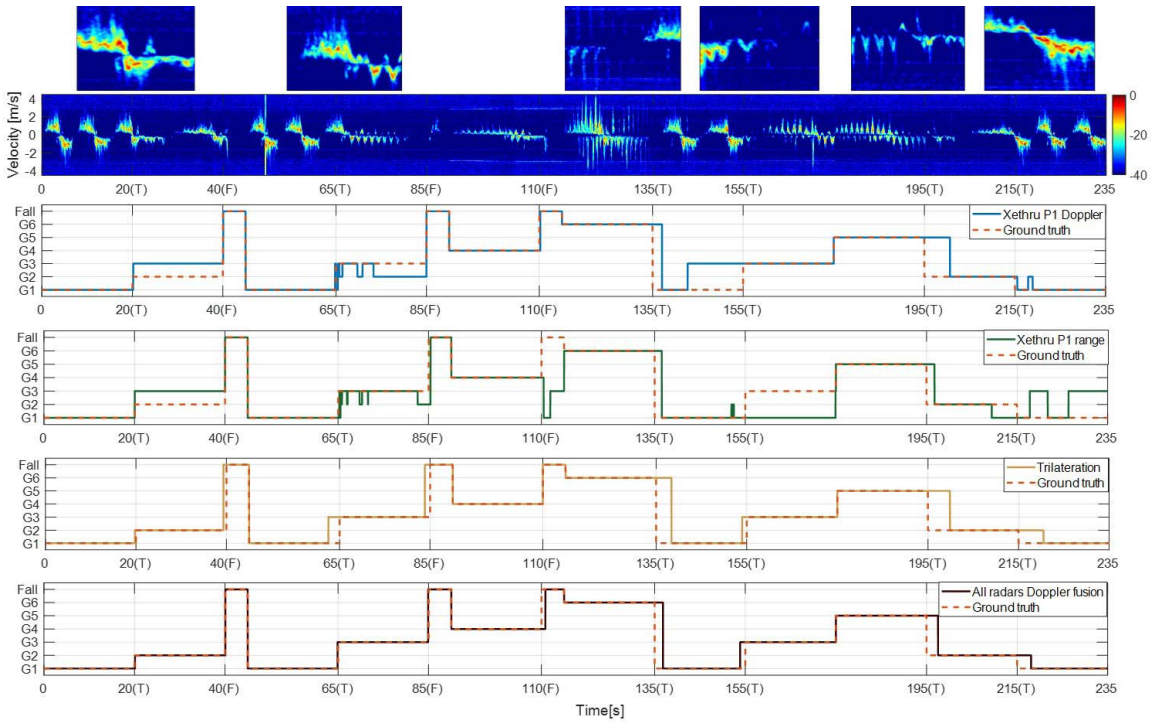

Fig. 16. Predictions vs ground truth for *sequential gaits* performed by a participant. From top to bottom: zoomed Doppler spectrogram of each gait transition; Doppler spectrogram for all sequential gaits recorded with Xethru P1; Xethru P1 results using Doppler; Xethru P1 results using range; signal level range fusion using trilateration; decision level Doppler fusion of all radar sensors. G1= normal walk; G2= slow walk; G3= dragging foot; G4= walk with cane; G5= walk with walker; G6= bunny jump; G7= controlled fall.

and +30% is attained for most participants via multi-radar trilateration. Fig. 12 shows the classification matrix for the results obtained using trilaterated coordinates as inputs to the Bi-LSTM network. Although the performance of trilateration decreases of 6%-9% for 'G9' to 'G11' compared to the micro-Doppler results, for the controlled fall detection trilateration outperforms micro-Doppler signature fusion. This justifies the benefits of exploring information fusion at different levels, i.e. signal level for range trilateration and decision level for micro-Doppler information used as networks' inputs.

IV. Data Processing for Sequential Gaits

In this section the analysis of sequential gaits is performed, i.e. gaits where there are natural and seamless transitions from one type of gait to the other that need to be accounted for in the classification. The efficacy of both usage of micro-Doppler and trilaterated range information as inputs to Bi-LSTM networks is demonstrated with experimental data.

Fig. 13 shows the classification results attained using *Doppler-BiLSTM* for sequential gaits. The Ancortek radar yields the highest mean classification accuracy of 85.4%, closely followed by the Xethru P1 at 84.8%. The side-looking Xethru P3 yields the lowest mean accuracy of 75%. Notably, participants #3 and #4 exhibit low classification accuracy across all sensors. The decision fusion between four radar systems with the NBC leads to an accuracy boost of +7.9% as compared to the best single radar, and improves significantly the minimum accuracy and standard deviation across participants as well.

Fig. 14 compares the classification performance using range information and trilaterated coordinates combining the data from the three Xethru radar P1-P2-P3. The range information from Xethru P1 yields about 83.7% mean accuracy across all participants, and trilateration yields approximately +7.3% performance improvement, even if this is less significant for some of the participants.

Fig. 15 shows the confusion matrix for the sequential gait classification results using Doppler information and decision fusion through a NBC. The confusion matrix has 7 classes for the 7 types of walking gaits contained in the sequences, including the fall. The main confusion can be observed between 'walking slowly' and 'dragging one foot', most likely because of the similarity between these walking patterns. Conversely, the recognition rate of the 'controlled fall' is even higher than that attained in the individual gait experiments.

A summarising example to compare the different proposed methods using both single sensors and fusion is shown in Figure 16. A time-synchronised spectrogram is provided for the entire sequence, composed by concatenating the 5 diverse sequential gait samples performed by a participant; 'T' and 'F' indicate the transition between individual gait types and fall events, respectively. Classification errors can appear as rapid oscillations of the classifier output (as between 65 and 85s for Xethru P1 using Doppler or range information in isolation), or as wrong decisions for long periods of time (e.g. at 20-40s for Xethru P1 using Doppler and at 155-175s for Xethru P1 using only range). In general, both approaches using range trilateration and using decision level fusion with Doppler information reduce the occurrence of these classification errors.

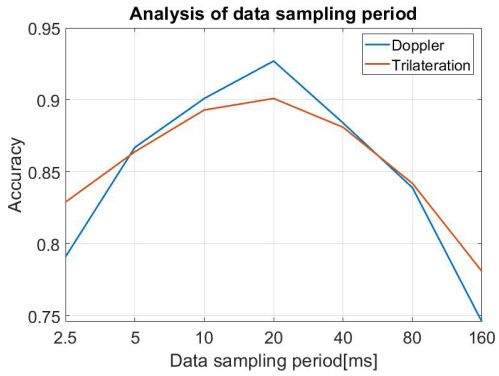

Fig. 17. The L1O classification accuracy with different data sampling periods for *sequential gaits*.

The remaining discrepancies between the ground-truth and the predictions concern time alignment: the correct classes (types of gaits) are predicted, but this can happen with up to several seconds of difference with respect to the time of the transition in the ground-truth.

In general, low signal strength received at one radar will lead to more classification errors. Thanks to the deployment geometry of the radars and the combination of their information via fusion approaches, there is no experimental area where the signal strength is too low at all radar sensors at the same time to yield acceptable classification performances.Furthermore, an analysis of the changes in classification accuracy with the length of data sampling period is shown in Figure 17. The original data sampling period for the gait data is about 20ms; we then re-sampled the sequential gaits data with a factor q. Different choices of this factor will lead to different data sampling period. In this paper, q is equal to $1/8$, $1/4$, $1/2$, 2, 4 and 8, whereas the corresponding data sampling period are 2.5, 5, 10, 40, 80 and 160ms. The Bi-LSTM network is used to test the re-sampled gait data comparing both Doppler and range information via trilateration. It is shown that the 'L1O' classification accuracy drops significantly if increasing or decreasing the original sampling period (20ms) of the radar data. Moreover, increasing the length of the data sampling period appears to lead to a more significant degradation compared to decreasing such parameter. Compared to the Doppler information (blue line), the trilaterated range information has a slower decrease rate, which suggests that fusion using trilateration algorithm can be more robust in terms of the ability of adapting to changes in the sampling period.

V. Conclusion and Future Work

This paper presented the classification of human gait patterns and falls in a radar sensors network composed of a FMCW radar and three UWB pulse radar placed at different spatial locations. The human gaits classified in this work are both individual and sequential, continuous gaits. These contain multiple walking styles performed one after the other, with natural transitions in between, including fall events developing from walking gait in certain cases.

Preliminary results obtained using conventional SVM and Random Forest classifiers are outperformed by the use of Bi-LSTM networks, capable of accounting for the temporal backward and forward correlations within the sequences of radar data. In terms of data fusion approaches, a signal level scheme based on trilateration to combine range information from different radar sensors proved to be very effective, and yielded comparable results to more conventional processing based on micro-Doppler. An experimental dataset with 14 participants and 12 walking gaits was used to validate the results. Decision fusion based on micro-Doppler information and the use of signal fusion based on range trilateration yielded approximately 98.2% and 95.2% classification accuracy, when applied on individual gaits. For sequential gait classification, the two approaches achieved 93% and 90%, respectively.

Future work will focus on different network architectures and components (e.g. Temporal Convolution Network and Connectionist Temporal Classification) for better modelling and learning sequential classification problems, as well as adding more participants and gait styles to the dataset, including totally unconstrained walking gait in any random direction. Cross-modality tests (training on fusion data and then test with single sensor) will be also important for evaluating the system performance under the worst-case of one sensor malfunctioning or being severely occluded by clutter in the environment. In addition, building a framework that combines the advantages of signal, feature and decision level fusion will be considered to subsequently improve the classification accuracy, especially for some gaits that cannot be easily classified via a single fusion approach.

Acknowledgment

The authors would like to acknowledge the participation of students of the Computational Intelligence for Radar (CI4R) Laboratory for the data collection, in particular, M. Mahbubur Rahman and A. Shrestha for their help.

References

[1] K. Chaccour, R. Darazi, A. H. El Hassani, and E. Andres, "From fall detection to fall prevention: A generic classification of fall-related systems," *IEEE Sensors J.*, vol. 17, no. 3, pp. 812–822, Feb. 2017.

[2] C. S. Florence, G. Bergen, A. Atherly, E. Burns, J. Stevens, and C. Drake, "Medical costs of fatal and nonfatal falls in older adults," *J. Amer. Geriatrics Soc.*, vol. 64, no. 4, pp. 693–698, 2018.

[3] S. C. Mukhopadhyay, "Wearable sensors for human activity monitoring: A review," *IEEE Sensors J.*, vol. 15, no. 3, pp. 1321–1330, Mar. 2015.

[4] A.-K. Seifert, M. G. Amin, and A. M. Zoubir, "Toward unobtrusive in-home gait analysis based on radar micro-Doppler signatures," *IEEE Trans. Biomed. Eng.*, vol. 66, no. 9, pp. 2629–2640, Sep. 2019.

[5] A.-K. Seifert, A. M. Zoubir, and M. G. Amin, "Detection of gait asymmetry using indoor Doppler radar," in *Proc. IEEE Radar Conf. (RadarConf)*, Apr. 2019, pp. 1–6.

[6] J. L. Kernec *et al.*, "Radar signal processing for sensing in assisted living: The challenges associated with real-time implementation of emerging algorithms," *IEEE Signal Process. Mag.*, vol. 36, no. 4, pp. 29–41, Jul. 2019.

[7] S. Z. Gurbuz and M. G. Amin, "Radar-based human-motion recognition with deep learning: Promising applications for indoor monitoring," *IEEE Signal Process. Mag.*, vol. 36, no. 4, pp. 16–28, Jul. 2019.

[8] T. R. Bennett, J. Wu, N. Kehtarnavaz, and R. Jafari, "Inertial measurement unit-based wearable computers for assisted living applications: A signal processing perspective," *IEEE Signal Process. Mag.*, vol. 33, no. 2, pp. 28–35, Mar. 2016.

[9] E. Cippitelli, F. Fioranelli, E. Gambi, and S. Spinsante, "Radar and RGB-depth sensors for fall detection: A review," *IEEE Sensors J.*, vol. 17, no. 12, pp. 3585–3604, Jun. 2017.

[10] C. Li *et al.*, "A review on recent progress of portable short-range noncontact microwave radar systems," *IEEE Trans. Microw. Theory Techn.*, vol. 65, no. 5, pp. 1692–1706, May 2017.

[11] J. A. Nanzer, "A review of microwave wireless techniques for human presence detection and classification," *IEEE Trans. Microw. Theory Techn.*, vol. 65, no. 5, pp. 1780–1794, May 2017.

[12] F. Fioranelli, J. L. Kernec, and S. A. Shah, "Radar for health care: Recognizing human activities and monitoring vital signs," *IEEE Potentials*, vol. 38, no. 4, pp. 16–23, Jul. 2019.

[13] B. Erol and M. G. Amin, "Radar data cube processing for human activity recognition using multisubspace learning," *IEEE Trans. Aerosp. Electron. Syst.*, vol. 55, no. 6, pp. 3617–3628, Dec. 2019.

[14] D. Tahmoush, "Review of micro-Doppler signatures," *IET Radar, Sonar Navigat.*, vol. 9, no. 9, pp. 1140–1146, Dec. 2015.

[15] Y. Kim and H. Ling, "Human activity classification based on micro-Doppler signatures using a support vector machine," *IEEE Trans. Geosci. Remote Sens.*, vol. 47, no. 5, pp. 1328–1337, May 2009.

[16] M. S. Seyfioglu, A. M. Ozbayoglu, and S. Z. Gürbüz, "Deep convolutional autoencoder for radar-based classification of similar aided and unaided human activities," *IEEE Trans. Aerosp. Electron. Syst.*, vol. 54, no. 4, pp. 1709–1723, Aug. 2018.

[17] Y. Kim and T. Moon, "Human detection and activity classification based on micro-Doppler signatures using deep convolutional neural networks," *IEEE Geosci. Remote Sens. Lett.*, vol. 13, no. 1, pp. 8–12, Jan. 2016.

[18] M. S. Seyfioglu, B. Erol, S. Z. Gurbuz, and M. G. Amin, "DNN transfer learning from diversified micro-Doppler for motion classification," *IEEE Trans. Aerosp. Electron. Syst.*, vol. 55, no. 5, pp. 2164–2180, Oct. 2019.

[19] S. Hochreiter and J. Schmidhuber, "Long short-term memory," *Neural Comput.*, vol. 9, no. 8, pp. 1735–1780, 1997.

[20] G. Klarenbeek, R. I. A. Harmanny, and L. Cifola, "Multi-target human gait classification using LSTM recurrent neural networks applied to micro-Doppler," in *Proc. Eur. Radar Conf. (EURAD)*, Nuremberg, Germany, Oct. 2017, pp. 167–170.

[21] M. Wang, G. Cui, X. Yang, and L. Kong, "Human body and limb motion recognition via stacked gated recurrent units network," *IET Radar, Sonar Navigat.*, vol. 12, no. 9, pp. 1046–1051, Sep. 2018.

[22] A. Graves and J. Schmidhuber, "Framewise phoneme classification with bidirectional LSTM and other neural network architectures," *Neural Netw.*, vol. 18, nos. 5–6, pp. 602–610, Jul. 2005.

[23] Z. Yu *et al.*, "Using bidirectional LSTM recurrent neural networks to learn high-level abstractions of sequential features for automated scoring of non-native spontaneous speech," in *Proc. IEEE Workshop Autom. Speech Recognit. Understand. (ASRU)*, Scottsdale, AZ, USA, Dec. 2015, pp. 338–345.

[24] M. Wang, Y. D. Zhang, and G. Cui, "Human motion recognition exploiting radar with stacked recurrent neural network," *Digit. Signal Process.*, vol. 87, pp. 125–131, Apr. 2019.

[25] C. Ding *et al.*, "Continuous human motion recognition with a dynamic range-Doppler trajectory method based on FMCW radar," *IEEE Trans. Geosci. Remote Sens.*, vol. 57, no. 9, pp. 6821–6831, Sep. 2019.

[26] H. Li, A. Shrestha, H. Heidari, J. L. Kernec, and F. Fioranelli, "Activities recognition and fall detection in continuous data streams using radar sensor," in *IEEE MTT-S Int. Microw. Symp. Dig.*, Nanjing, China, May 2019, pp. 1–4.

[27] H. Li, A. Shrestha, H. Heidari, J. L. Kernec, and F. Fioranelli, "Bi-LSTM network for multimodal continuous human activity recognition and fall detection," *IEEE Sensors J.*, vol. 20, no. 3, pp. 1191–1201, Feb. 2020.

[28] A. Shrestha, H. Li, J. L. Kernec, and F. Fioranelli, "Continuous human activity classification from FMCW radar with bi-LSTM networks," *IEEE Sensors J.*, vol. 20, no. 22, pp. 13607–13619, Nov. 2020.

[29] F. Wang, M. Skubic, M. Rantz, and P. E. Cuddihy, "Quantitative gait measurement with pulse-Doppler radar for passive in-home gait assessment," *IEEE Trans. Biomed. Eng.*, vol. 61, no. 9, pp. 2434–2443, Sep. 2014.

[30] H. Li, A. Shrestha, H. Heidari, J. L. Kernec, and F. Fioranelli, "A multisensory approach for remote health monitoring of older people," *IEEE J. Electromagn., RF Microw. Med. Biol.*, vol. 2, no. 2, pp. 102–108, Jun. 2018.

[31] H. Li, A. Shrestha, H. Heidari, J. L. Kernec, and F. Fioranelli, "Magnetic and radar sensing for multimodal remote health monitoring," *IEEE Sensors J.*, vol. 19, no. 20, pp. 8979–8989, Oct. 2019.

[32] R. C. King, E. Villeneuve, R. J. White, R. S. Sherratt, W. Holderbaum, and W. S. Harwin, "Application of data fusion techniques and technologies for wearable health monitoring," *Med. Eng. Phys.*, vol. 42, pp. 1–12, Apr. 2017.

[33] X. Bai, Y. Hui, L. Wang, and F. Zhou, "Radar-based human gait recognition using dual-channel deep convolutional neural network," *IEEE Trans. Geosci. Remote Sens.*, vol. 57, no. 12, pp. 9767–9778, Dec. 2019.

[34] F. Luo, S. Poslad, and E. Bodanese, "Human activity detection and coarse localization outdoors using micro-Doppler signatures," *IEEE Sensors J.*, vol. 19, no. 18, pp. 8079–8094, Sep. 2019.

[35] S. Z. Gürbüz, B. Erol, B. Çağlıyan, and B. Tekeli, "Operational assessment and adaptive selection of micro-Doppler features," *IET Radar, Sonar Navigat.*, vol. 9, no. 9, pp. 1196–1204, Dec. 2015.

[36] P. Lei, Y. Zhang, J. Wang, and J. Sun, "Estimation of human gait cycle based on cepstrum of radar micro-Doppler signatures," in *Proc. Prog. Electromagn. Res. Symp. Fall (PIERS-FALL)*, Singapore, Nov. 2017, pp. 2356–2359.

[37] R. I. A. Harmanny, J. J. M. D. Wit, and G. P. Cabic, "Radar micro-Doppler feature extraction using the spectrogram and the cepstrogram," in *Proc. 11th Eur. Radar Conf.*, Rome, Italy, Oct. 2014, pp. 165–168.

[38] C. Karabacak, S. Z. Gurbuz, A. C. Gurbuz, M. B. Guldogan, G. Hendeby, and F. Gustafsson, "Knowledge exploitation for human micro-Doppler classification," *IEEE Geosci. Remote Sens. Lett.*, vol. 12, no. 10, pp. 2125–2129, Oct. 2015.

[39] L. I. Kuncheva and J. J. Rodríguez, "A weighted voting framework for classifiers ensembles," *Knowl. Inf. Syst.*, vol. 38, no. 2, pp. 259–275, Feb. 2014.

[40] A. Graves, A.-R. Mohamed, and G. Hinton, "Speech recognition with deep recurrent neural networks," in *Proc. IEEE Int. Conf. Acoust., Speech Signal Process.*, May 2013, pp. 6645–6649.

[41] X. Li, Y. He, Y. Yang, Y. Hong, and X. Jing, "LSTM based human activity classification on radar range profile," in *Proc. IEEE Int. Conf. Comput. Electromagn. (ICCEM)*, Shanghai, China, Mar. 2019, pp. 1–2.

[42] Z. Zeng, M. G. Amin, and T. Shan, "Automatic arm motion recognition based on radar micro-Doppler signature envelopes," *IEEE Sensors J.*, vol. 20, no. 22, pp. 13523–13532, Nov. 2020.

[43] M. G. Amin, Z. Zeng, and T. Shan, "Hand gesture recognition based on radar micro-Doppler signature envelopes," in *Proc. IEEE Radar Conf. (RadarConf)*, Boston, MA, USA, Apr. 2019, pp. 1–6.

[44] F. Fioranelli, M. Ritchie, and H. Griffiths, "Performance analysis of centroid and SVD features for personnel recognition using multistatic micro-Doppler," *IEEE Geosci. Remote Sens. Lett.*, vol. 13, no. 5, pp. 725–729, May 2016.

[45] S. M. Kay, *Fundamentals of Statistical Signal Processing*. Upper Saddle River, NJ, USA: Prentice-Hall PTR, 1993.

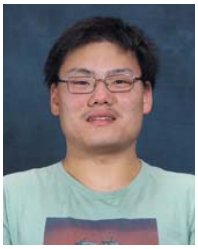

Haobo Li (Member, IEEE) received the B.Eng. degree in electrical and electronic engineering from Northumbria University at Newcastle in 2015, and the M.S. degree in communication and signal processing from the University of Newcastle in 2016. He is currently pursuing the Ph.D. degree with the School of Engineering, University of Glasgow. He is working on information fusion of multiple sensing technologies for assisted living applications and gesture recognition.

Ajay Mehul is currently pursuing the B.S. degree in computer science with the University of Alabama (UA). His research focuses on human–computer interaction with the HTIL Lab, UA, where he is developing software tools aiding research with the CI4R Lab.

Julien Le Kernec (Senior Member, IEEE) received the B.Eng. and M.Eng. degrees in electronic engineering from the Cork Institute of Technology, Ireland, in 2004 and 2006, respectively, and the Ph.D. degree in electronic engineering from University Pierre and Marie Curie, France, in 2011. He is currently a Senior Lecturer with the School of Engineering, University of Glasgow. He is also a Senior Lecturer with the University of Electronic Science and Technology of China and an Adjunct Associate Professor with the ETIS Laboratory, University of Cergy-Pontoise, France. His research interests include radar system design, software-defined radio/radar, signal processing, and health applications.

Sevgi Z. Gurbuz (Senior Member, IEEE) received the B.S. degree in electrical engineering with minor in mechanical engineering and the M.Eng. degree in electrical engineering and computer science from the Massachusetts Institute of Technology, Cambridge, MA, USA, in 1998 and 2000, respectively, and the Ph.D. degree in electrical and computer engineering from the Georgia Institute of Technology, Atlanta, GA, USA, in 2009. From February 2000 to January 2004, she worked as a Radar Signal Processing Research Engineer with the U.S. Air Force Research Laboratory, Sensors Directorate, Rome, NY, USA. She was an Assistant Professor with the Department of Electrical-Electronics Engineering, TOBB University, Ankara, Turkey, and a Senior Research Scientist with the TUBITAK Space Technologies Research Institute, Ankara. She is currently an Assistant Professor with the Department of Electrical and Computer Engineering, University of Alabama at Tuscaloosa. Her current research interests include radar signal processing, physics-aware machine learning, human motion recognition for biomedical, vehicular autonomy, human–computer interaction (HCI) applications, and sensor networks. Dr. Gurbuz was a recipient of the 2020 SPIE Rising Researcher Award, the EU Marie Curie Research Fellowship, and the 2010 IEEE Radar Conference Best Student Paper Award.

Francesco Fioranelli (Senior Member, IEEE) received the Ph.D. degree from Durham University, U.K., in 2014. He was a Postdoctoral Research Associate at University College London from 2014 to 2016, prior to joining the University of Glasgow. He is currently a TT Assistant Professor with the Department of Microelectronics, Delft University of Technology. His research interests include development of radar systems and radar signal processing for applications, including human signatures analysis for healthcare and security, drones and UAVs detection and classification, automotive radar, wind farm, and sea clutter characterization. Dr. Fioranelli is a Chartered Engineer (C.Eng.) through the IET, and regularly acts as a reviewer for academic journals in the domain of radar sensing, such as IEEE TRANSACTIONS ON AEROSPACE AND ELECTRONIC SYSTEMS, IEEE SENSORS, IEEE TRANSACTIONS ON GEOSCIENCE AND REMOTE SENSING, and *IET Radar, Sonar and Navigation*.